catalysts

MDPI

Article

Sustainable Hydrogen Production from Starch Aqueous Suspensions over a $Cd_{0.7}Zn_{0.3}S$-Based Photocatalyst

Anna Y. Kurenkova, Tatiana B. Medvedeva, Nikolay V. Gromov, Andrey V. Bukhtiyarov, Evgeny Y. Gerasimov, Svetlana V. Cherepanova and Ekaterina A. Kozlova *

Federal Research Center Boreskov Institute of Catalysis SB RAS, Lavrentieva Ave. 5, 630090 Novosibirsk, Russia; kurenkova@catalysis.ru (A.Y.K.); tanmedvedeva@catalysis.ru (T.B.M.); gromov@catalysis.ru (N.V.G.); avb@catalysis.ru (A.V.B.); gerasimov@catalysis.ru (E.Y.G.); svch@catalysis.ru (S.V.C.)
* Correspondence: kozlova@catalysis.ru; Tel.: +7-383-3269-543

Abstract: We explored the photoreforming of rice and corn starch with simultaneous hydrogen production over a $Cd_{0.7}Zn_{0.3}S$-based photocatalyst under visible light irradiation. The photocatalyst was characterized by UV–vis diffuse reflectance spectroscopy, X-ray diffraction, and X-ray photoelectron spectroscopy. The influence of starch pretreatment conditions, such as hydrolysis temperature and alkaline concentration, on the reaction rate was studied. The maximum rate of H_2 evolution was 730 $\mu mol \cdot h^{-1} \cdot g^{-1}$, with AQE = 1.8% at 450 nm, in the solution obtained after starch hydrolysis in 5 M NaOH at 70 °C. The composition of the aqueous phase of the suspension before and after the photocatalytic reaction was studied via high-performance liquid chromatography, and such products as glucose and sodium gluconate, acetate, formate, glycolate, and lactate were found after the photocatalytic reaction.

Keywords: photocatalysis; hydrogen production; cadmium sulfide; zinc sulfide; starch hydrolysis; visible light; photoreforming

Citation: Kurenkova, A.Y.; Medvedeva, T.B.; Gromov, N.V.; Bukhtiyarov, A.V.; Gerasimov, E.Y.; Cherepanova, S.V.; Kozlova, E.A. Sustainable Hydrogen Production from Starch Aqueous Suspensions over $Cd_{0.7}Zn_{0.3}S$-Based Photocatalyst. *Catalysts* **2021**, *11*, 870. https://doi.org/10.3390/catal11070870

Academic Editor: Rufino M. Navarro Yerga

Received: 31 May 2021
Accepted: 19 July 2021
Published: 20 July 2021

1. Introduction

One of the problems facing humanity is the rapid increase in greenhouse gas concentrations in the atmosphere. The main cause is fossil-fuel combustion, which is responsible for the release of the most significant greenhouse gas—carbon dioxide [1]. To overcome this problem, the development of alternative energy sources is necessary. Hydrogen is considered a prospective energy source for the future, as it combines the following benefits: high heating value, environmentally friendly combustion product, and the abundance of hydrogen on the Earth. Most of the hydrogen being produced is obtained from fossil fuels, which cannot be considered a sustainable method because of their limited abundance and because of CO_2 production [1,2]. Biomass also contains great amounts of hydrogen, which can be extracted in several ways. Nowadays, the most used methods are thermochemical processes, such as the pyrolysis and gasification of biomass [3,4]. Both of these require a high temperature, but more importantly, they produce greenhouse gases as byproducts. Therefore, the development of alternative energy sources to produce pure hydrogen under ambient conditions is necessary.

One of the more promising ways to produce hydrogen from biomass is the photocatalytic reforming of plant biomass. Soluble biomass derivatives, such as sugars, alcohols, and carboxylic acids, have been widely studied as substrates in hydrogen evolution reaction [5–11]. A wide range of valuable organic compounds have been found in reaction solutions after photocatalytic reforming, such as formic acid [12], acetic acid [13–15], acetaldehyde, ethanol, acetol, methanol, and glycolaldehyde [16–18]. It has been concluded that the nature of the photocatalyst, its activity, and the light source all affect product formation [9]. However, raw biomass components, such as cellulose, lignin, and starch,

look more promising from the economical and practical points of view. In these cases, biomass could be converted into valuable products via a simpler one-stage technique, without any pretreatment for the separation of soluble compounds, which would require additional costs. Despite this, studies on raw biomass component photoreforming are limited. Moreover, most of them are devoted to the photoreforming of lignocellulose under UV light irradiation [19], which makes up only 4% of solar radiation, while visible light contributes about 46% [20]. Furthermore, the photoreforming of insoluble components under visible light irradiation [21] and under simulated [22–26] or natural [27] solar light has been performed in few works; therefore, the approach using biomass and solar light to obtain hydrogen is promising, and worthy of detailed study. Among biomass-derived substrates, starch is one of the least studied, despite being the main polymer of some plants, for example, corn, rice, and potato [28,29].

The CdS-based photocatalyst is one of the most promising semiconductors for hydrogen evolution because the bandgap energy of CdS is about 2.4 eV, which allows visible light irradiation to be absorbed by the photocatalyst [30]. Once the light is absorbed, the semiconductor generates e^-/h^+ pairs, then electrons reduce H^+ and holes oxidize the substrate on the surface of the semiconductor [31]. The toxicity of Cd^{2+} cations is quite high; however, the solubility constant of CdS is very low (1.6×10^{-28}). In our previous research, the absence of toxic effects in eukaryotic cells and nematodes was demonstrated [32]. The main problem is the recombination of photogenerated charge carriers, which suppresses the reaction efficiency and hydrogen evolution rate [33]. In our previous works, multiphase photocatalysts based on a solid sulfide solution of cadmium, zinc, and zinc sulfide ($Cd_{1-x}Zn_xS$/ZnS) and with deposited platinum or gold particles showed high reactivity in hydrogen evolution reactions using different organic and inorganic electron donors [34–36]. The deposition of metals facilitates efficient charge separation, thereby improving the rate of hydrogen evolution [37]. Platinum is usually used as a co-catalyst, as this metal not only possesses a high value of work function [38], but also promotes the adsorption of organic substances, thereby providing a higher rate of hydrogen evolution than other metals [39,40]. Our study of hydrogen evolution from a cellulose suspension showed that the photocatalyst with 0.5 wt.% platinum had the highest activity [35].

Based on the above, the present work aimed to investigate the hydrogen evolution reaction using starch as a substrate over platinized $Cd_{0.7}Zn_{0.3}S$/ZnS (0.5 wt.% of Pt) under visible light. We studied the influence of the starch and NaOH concentration, the temperature of the starch pretreatment (70–140 °C), and the photocatalyst concentration on the reaction rate. A thorough analysis of the organic products formed from starch under different pretreatment conditions was conducted. Additionally, the composition of the soluble organic products following photocatalytic hydrogen production from aqueous suspensions of corn starch was determined for the first time. It has been shown that a simple pretreatment in combination with photocatalysis makes it possible to obtain hydrogen and valuable organic compounds from practically insoluble starch.

2. Results and Discussion

2.1. Photocatalyst Characterization

Different characterization techniques were applied to investigate the synthesized photocatalyst. The phase structure of the solid sulfide solution was studied via the XRD method. The XRD pattern is shown in Figure 1a, and it demonstrates three broad peaks. The last two peaks were fitted using the Rietveld method via two phases: ZnS and $Cd_{1-x}Zn_xS$ [41]. As shown in Figure 1a, there is good agreement between the curve based on data obtained and the calculated curve. The x parameter in $Cd_{1-x}Zn_xS$ and the lattice parameters were determined using the Vegard rule; the reference points were ZnS (PDF # 05-0566, lattice constant a = 5.406 Å) and CdS (PDF # 42-1411, lattice constant a = 5.818 Å) with a cubic structure. It was shown that the sample consists of two phases: a $Cd_{0.7}Zn_{0.3}S$

solid sulfide solution with a lattice parameter equal to 5.70 Å and $Zn_{0.95}Cd_{0.05}S$ with a lattice parameter equal to 5.43 Å. The average crystalline size for both phases was 3.8 nm.

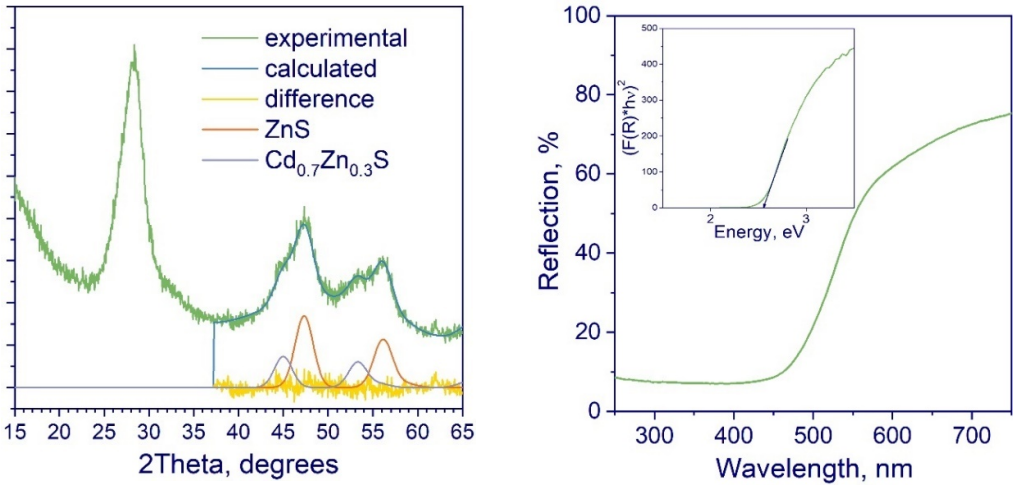

(**a**) (**b**)

Figure 1. X-ray diffraction (XRD) pattern with the deconvolution of the two last peaks (**a**) and diffuse reflectance spectrum with the Tauc plot (**b**) of the synthesized sample.

Further, we will denote the sample in the text as $Cd_{0.7}Zn_{0.3}S$/ZnS. The characteristic peaks of platinum were not detected in the XRD pattern, probably because of the low metal content (0.5 wt.%).

To study the optical properties of the photocatalyst, the UV–vis spectrum was obtained (Figure 1b). The band gap energy was calculated using the Tauc function for direct semiconductors $F(R)^2 (h\nu)^2$ and the value was 2.55 eV. The adsorption edge of the photocatalyst was about 480 nm, which means the photocatalyst is able to absorb visible light irradiation with λ = 450 nm.

The surface chemical composition was studied via the XPS technique (Figure 2). The Pt*4f* binding energy was 72.8 eV, which corresponds to platinum in the oxidized state (Pt^{2+} in PtO oxide) [42,43]. The binding energies of Cd $3d_{5/2}$, Zn $2p_{3/2}$, and S $2p_{3/2}$ were 405.4, 1022.3, and 161.8 eV, respectively, which are typical of cadmium and zinc sulfides. No other ions were identified by the XPS method [44–47].

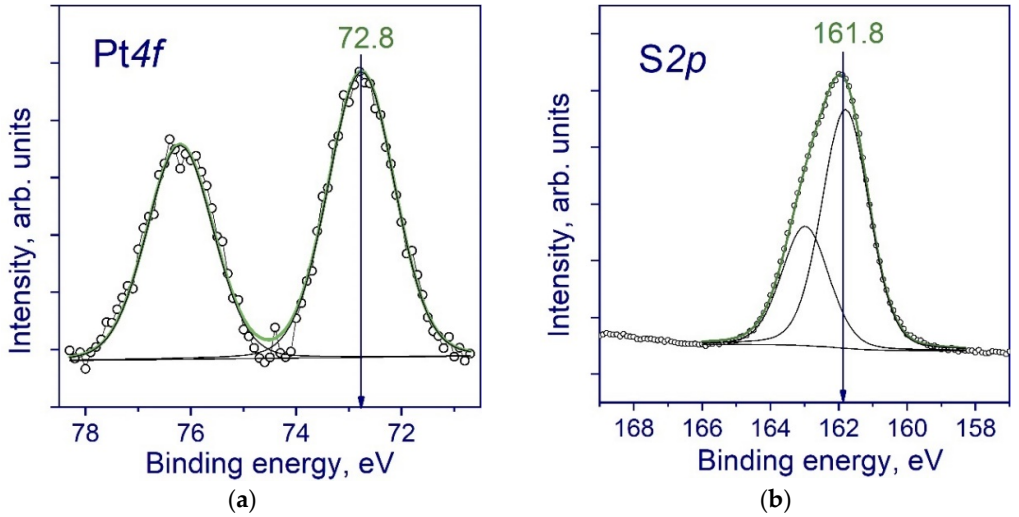

(**a**) (**b**)

Figure 2. The Pt *4f* (**a**) and S*2p* (**b**) X-ray photoelectron spectroscopy (XPS) spectra of the synthesized photocatalyst.

To elucidate the structure of the composites, we obtained TEM images as well as HAADF-STEM images with EDX elemental mapping of the synthesized photocatalyst (Figure 3). Figure 3a,b shows that the sample has a disordered structure with coherently scattering domains about 5 nm, which is in good accordance with the XRD results. Note that platinum nanoparticles are not visible in TEM images, likely because of a very small size. However, elemental mapping (Figure 3c) shows the presence of platinum evenly distributed over the surface of the composite sample. The elemental distribution of cadmium and zinc shows that aggregates of cadmium-enriched and zinc-enriched phases with a size of 100–500 nm are formed. These aggregates are in close contact, which should ensure the effective formation of interfacial heterojunctions that provide high photocatalytic activity.

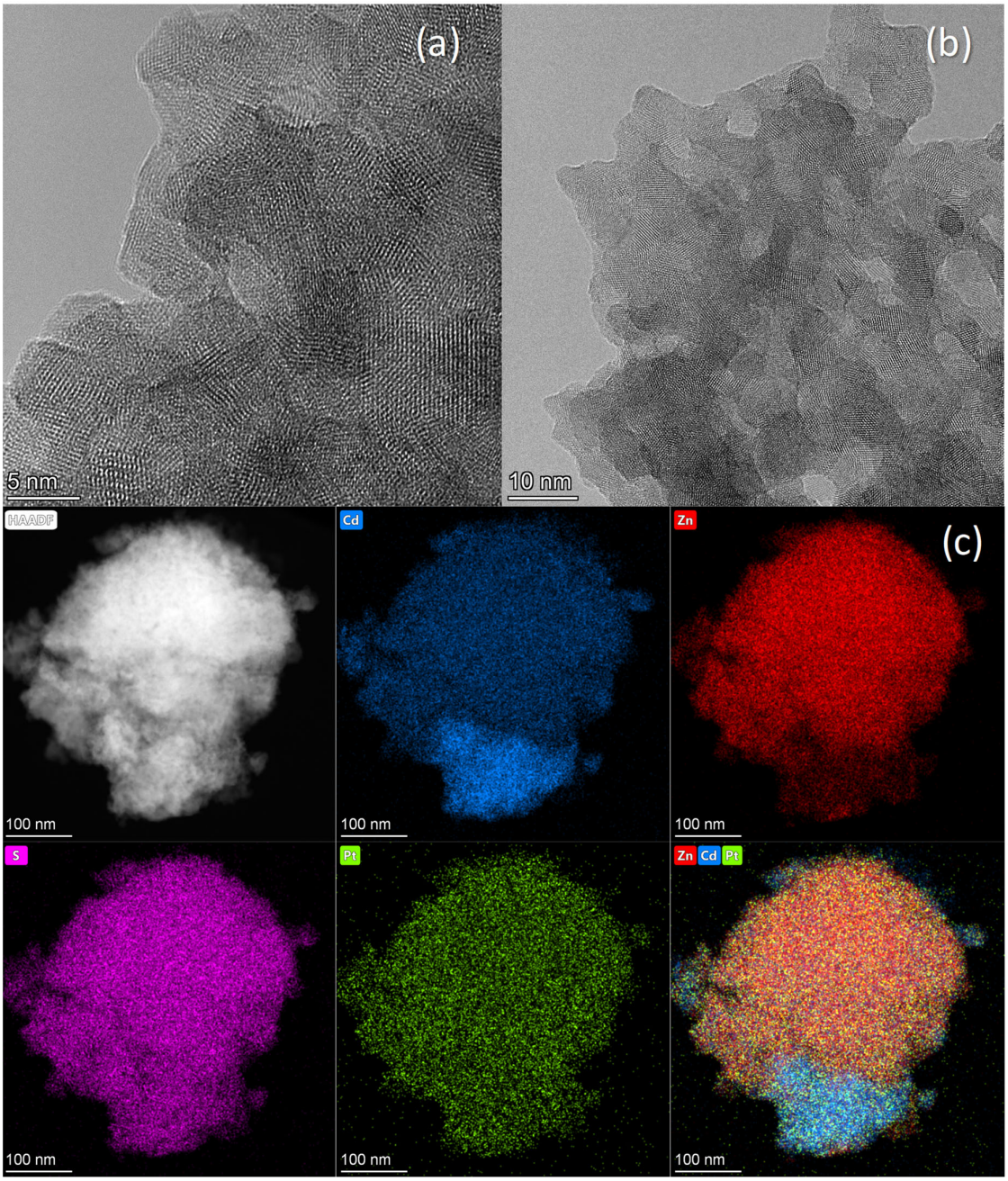

Figure 3. (**a**,**b**) HRTEM and (**c**) HAADF-STEM images with EDX with elemental mapping of the synthesized sample.

Following the photocatalyst's characterization, we can conclude that the photocatalyst has a multiphase structure $PtO_x/Cd_{0.7}Zn_{0.3}S/ZnS$, which benefits photocatalytic hydrogen production via enhanced charge separation [48].

2.2. Photocatalytic Activity

At the beginning, we tested rice and corn starch as substrates to find out the most active substrate for hydrogen evolution. In preliminary experiments, it was shown that the amount of hydrogen evolved without using a substrate is negligible. The dependence of the yield of H_2 (t = 2 h) on starch concentration is shown in Figure 4a. The dependence has a weakly expressed maximum equal to 50.8 μmol at a concentration of starch of 5 $g \cdot L^{-1}$. The decrease in activity at high starch contents is related to the obstructed light penetration caused by a high content of starch particles in the reaction suspension. Although the yields of H_2 with different substrates were similar, corn starch was more active at 5 $g \cdot L^{-1}$ and was chosen for further experiments.

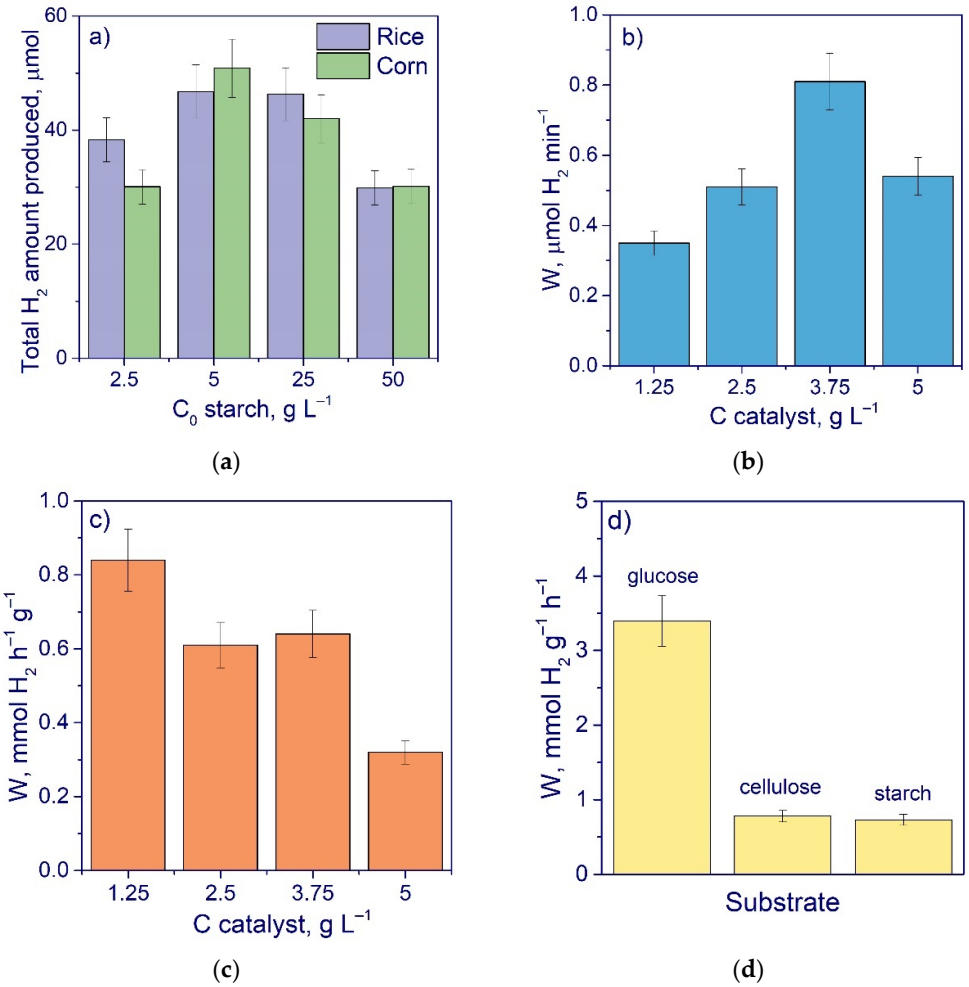

Figure 4. (**a**) The dependence of total H_2 amount on starch content; (**b**) the dependence of H_2 evolution rate on catalyst concentration, corn starch; (**c**) the dependence of specific activity on the catalyst concentration, corn starch; and (**d**) comparison of the rate of H_2 evolution from different biomass substrates over a $Cd_{1-x}Zn_xS$-based photocatalyst. Conditions: C_0(NaOH) = 5 M, C_0(starch) = 5 $g \cdot L^{-1}$, C(cat) = 2.5 $g \cdot L^{-1}$ unless otherwise stated, V = 20 mL, λ = 450 nm, t(reaction) = 120 min.

Another potential reason for the obstructed light penetration may be the high concentration of photocatalyst [49]. On the other hand, the increase in photocatalyst should

lead to the enhancement of activity, given the increased amount of active centers for H_2 evolution. As such, it is important to establish the optimum catalyst loading [50]. Figure 4b shows the dependence of the rate of H_2 formation on photocatalyst concentration. The rate increases linearly, reaching the maximum at the concentration of 3.75 $g \cdot L^{-1}$, and then falls. The specific rate of hydrogen evolution per gram of photocatalyst, presented in Figure 4c, reaches its maximum at the lowest catalyst loading of 1.25 $g \cdot L^{-1}$. For further experiments, the concentration of 2.5 $g \cdot L^{-1}$ was chosen, as it provides the optimum combination of absolute and specific rates of H_2 formation.

It is known the plant biomass undergoes hydrolysis under alkaline conditions [51]. This effect is beneficial for photocatalysis as soluble organic compounds can be easily absorbed onto the photocatalyst's surface and thus react with the photogenerated charge carriers [52]. Therefore, at the next stage, we studied the influence of sodium hydroxide concentration on the reaction rate (Figure 5a). The increase in NaOH concentration led to enhanced H_2 evolution. The highest reaction rate achieved in the 5 M solution of NaOH was equal to 535 ± 50 $\mu mol \cdot h^{-1} \cdot g^{-1}$, with an AQE = 1.3%. It should be noted that this kinetic curve reached a plateau after 2 h of irradiation, and the total amount of H_2 produced was similar to the amount of H_2 that evolved from 1 M NaOH solution after 6 h of irradiation. In the absence of NaOH, the amount of H_2 detected was close to zero. We can thus conclude that starch can be hydrolyzed to a limited extent, even in a high-alkaline environment, and long-term effective H_2 evolution cannot be guaranteed.

Another method described in the literature for starch dissolution is the thermal treatment of the starch aqueous solution [23]. As such, the next series of kinetic experiments was devoted to alkaline hydrolysis under heat treatment, with the temperature varying in the range of 70–140 °C. The same concentrations (0.1 M, 1 M, and 5 M) of NaOH were applied. At 70 °C, transparent solutions were obtained from 1 M and 5 M suspensions of NaOH after several minutes of stirring, while when 0.1 M NaOH was used, full starch dissolution was not achieved even after 1 h. At 105 and 140, transparent yellow solutions were obtained in the cases of 0.1 M and 1 M NaOH solutions.

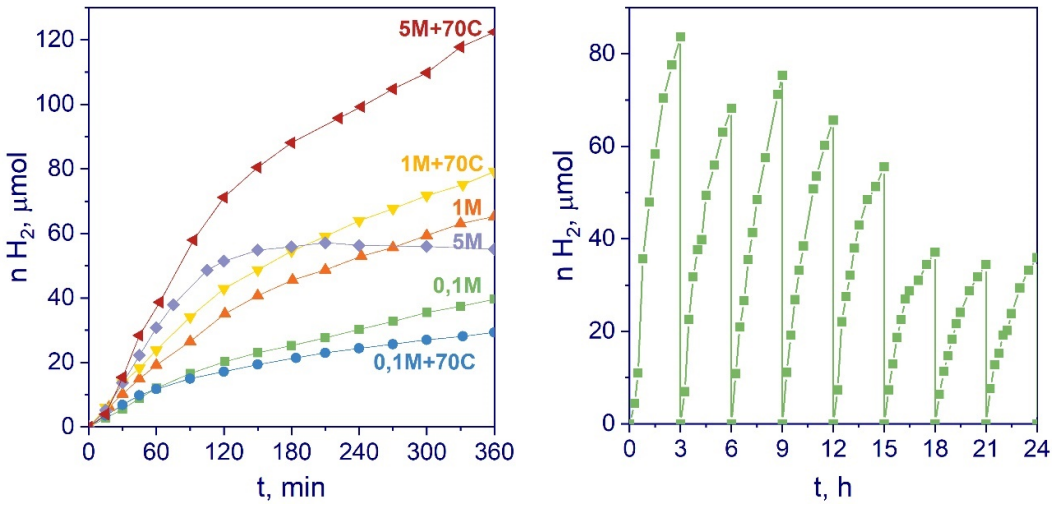

Figure 5. (**a**) The kinetic curves of H_2 evolution from corn starch aqueous suspensions at different NaOH concentrations, with pretreatment at 70 °C and without pretreatment. Conditions: C_0(starch) = 5 $g \cdot L^{-1}$, C(cat) = 2.5 $g \cdot L^{-1}$, V = 20 mL, λ = 450 nm, T = 20 °C; (**b**) the yield of H_2 during consecutive photocatalytic runs. C_0(starch) = 5 $g \cdot L^{-1}$, C(cat) = 2.5 $g \cdot L^{-1}$, C_0(NaOH) = 5 M, V = 20 mL, λ = 450 nm, T(starch pretreatment) = 70 °C.

Figure 5a demonstrates the kinetic curves of hydrogen evolution in two series of experiments—without preliminary heating treatment and with heating treatment at 70 °C. When we used a higher temperature (105 °C and 140 °C) for starch pretreatment, only a

small amount of H_2 was produced after 6 h of irradiation, and these results are not shown. Additionally, no hydrogen evolved from the starch aqueous suspension after heating at 70 °C without NaOH. On the contrary, heat-pretreating starch at 70 °C with a high alkaline concentration (1 or 5 M) led to an increase in the hydrogen evolution rate. We should note that the kinetic curve of H_2 evolution from starch treated at 5 M NaOH and 70 °C does not reach a plateau even after 6 h of irradiation. The rate of H_2 evolution for the first 2 h was 730 $h^{-1} \cdot g^{-1}$, with AQE = 1.8% (450 nm); for the next 4 h, these values were 240 $\mu mol \cdot h^{-1} \cdot g^{-1}$ and 0.6%, respectively. The comparison of these results with data in the literature is given in Table 1. The rate of H_2 evolution and the AQE obtained in this study in most cases are higher in comparison with the activity of other systems, including that of raw biomass substrate. Moreover, this is one of the first studies on the photocatalytic production of H_2 from insoluble starch. Additionally, the formation of H_2 from starch was compared to the results obtained using glucose solutions, or α-cellulose suspension, as substrates for H_2 production over the platinized $Cd_{1-x}Zn_xS$ photocatalysts, under the same conditions (Figure ~~43~~d) [34,35]. The rates of H_2 evolution from different polymers of glucose—cellulose and corn starch—are the same, whereas the rate in the case of the use of glucose is 3.5 times higher. This effect is likely related to the high solubility of glucose. Despite the high complexity of the raw biomass substrate, the developed photocatalyst achieved comparable rates of H_2 production.

Sulfide-based photocatalysts are prone to photocorrosion [34]. The stability of the synthesized photocatalyst was investigated during eight 3 h runs (Figure 5b). After each run, the photocatalytic reactor was purged with argon. The dependence of H_2 yield on time is clearly complicated; this may be caused by the complexity of the substrate. However, the rate of H_2 evolution was reasonably high during the first 18 h, then the rate decreased in every run, but stayed constant for the last 9 h of the experiment. The total yield of H_2 over 24 h was 460 μmol.

Table 1. Comparison of H_2 evolution rate from raw biomass substrate.

Photocatalyst	Substrate	Light Source	W, μmol $H_2 \cdot h^{-1} \cdot g^{-1}$	AQE, %	Reference
CN_x	xylan	AM 1.5G, 100 mW cm^{-2}	137	-	**Error! Reference source not found.**
	lignin		40.8	-	
0.32%Pt/TiO_2	rice husks	Natural sunlight, 45 mW cm^{-2}	95	-	27
5%Pt/TiO_2	potato	Xe, 500 mW cm^{-2}	13	-	9
	seaweed		25	-	
	chlorella		90	-	
	rice plant		8	-	
0.1%Pt/TiO_2	starch	Solar Box 1500e, 500 W m^{-2}	806	3.28	23
0.25%Pt/o-g-C_3N_4			593	0.54	
CdS/CdO_x	lignin	AM 1.5G, 100 mW cm^{-2}	260	-	22
	bagasse		650	-	
3%Au/CdS	soluble starch	Xe, cut filter (λ > 450 nm)	20	-	58
$PtO_x/Cd_{0.7}Zn_{0.3}S$/ZnS	corn starch	LED 450 nm, 14 mW cm^{-2}	730	1.8	This study

Taking into account the results of the kinetic experiments, the combination of an alkaline environment with heating clearly contributes to efficient starch hydrolysis, with the release of soluble organic compounds. These compounds can act as electron donors and react with photogenerated charge carriers to form oxidized derivatives [53]. On the other hand, the dependence of H_2 evolution rate on hydrolysis temperature reached a

maximum at 70 °C, and it was shown that, after starch pretreatment at 105 °C and 140 °C, the obtained hydrolysates were not effective substrates for H_2 formation.

To clarify the reasons for this effect, we studied the composition of the aqueous phase of the reaction mixture at different pretreatment temperatures. The reaction suspension was filtered out and analyzed via HPLC. We analyzed the composition of the soluble organic compounds in suspensions of starch heated in 0.1 M and 1 M NaOH at different temperatures (70 °C, 105 °C, and 140 °C) before and after the photocatalytic reaction. The aqueous phase of the suspension with 5 M NaOH was not studied, as a solution with such a high concentration of NaOH is not possible for HPLC. Table 2 outlines the composition of the aqueous phases of the reaction suspensions before and after photocatalytic H_2 evolution. Only a trace amount of glucose was found in the alkaline (0.1 M or 1 M NaOH) suspension before the reaction without heat treatment owing to the negligible dissolution of the starch. After the photocatalytic production of hydrogen from untreated starch suspensions, glucose and other organic substances were found in the solution, indicating the simultaneous hydrolysis of starch and the oxidation of the hydrolysis products through photocatalytic reaction. Table 2 shows that the heating of a starch alkaline suspension at 70 °C resulted in the hydrolysis of the starch, with the formation of glucose as a product. After carrying out the photocatalytic reaction of hydrogen evolution, the glucose concentration increased; moreover, additional valuable organic products, including lactate and gluconate, were detected. In the case of hydrolysis at 105 °C and 140 °C, no glucose was detected in the solutions either before or after the reaction; the solutions contain mostly formate, lactate, and acetate anions. Additionally, the rate of hydrogen evolution was close to zero, and the concentration of the detected organic compounds remained almost constant before and after the reaction. It should be noted that the formate concentration increased with the hydrolysis temperature (Table 2), while the content of more complex organic compounds decreased. Thus, the increase in temperature facilitates the further alkaline hydrolysis of starch, and results in the formation of simple organic compounds, which are not effective substrates for H_2 evolution over a sulfide-based photocatalyst.

As such, the alkaline hydrolysis of starch at 70 °C facilitates the best composition of a reaction solution for H_2 evolution. With the increase in the pretreatment temperature, the content of simple organic compounds increased. In contrast, the relative concentration of glucose decreased. Figure 6 shows the relative distributions of the organic compounds detected in the solutions after the H_2 evolution reaction. One can see that two factors affect the scope of organic compound transformation: alkali concentration and hydrolysis temperature. During the photocatalytic reaction, glucose transforms into valuable organic products, such as gluconic and glycolic acids.

Table 2. The results of aqueous phase analysis. C_0(corn starch) = 5 g·L^{-1}, C(cat) = 2.5 g·L^{-1}, V = 20 mL. TOC—total organic carbon.

N of Filtrate	C_0 NaOH, M	Heating Temperature	Organic Compounds Detected	Concentration, mM·L^{-1}	TOC, g L^{-1}
1 *	0.1	-	glucose	trace	0.10
1	0.1	-	glucose	0.38	0.21
			acetate	0.42	
			glycolate	0.04	
			lactate	0.04	
			gluconate	trace	
2 *	0.1	70 °C	glucose	0.06	0.80
2	0.1	70 °C	glucose	0.4	1.38
			acetate	0.18	
			glycolate	0.2	
			lactate	0.09	

			gluconate	trace	
			formate	0.81	
3 *	1.0	-	glucose	trace	2.58
3	1.0	-	glucose	0.43	3.12
			acetate	0.36	
			glycolate	0.21	
			gluconate	trace	
4 *	1.0	70 °C	glucose	0.09	3.19
4	1.0	70 °C	glucose	0.54	3.04
			acetate	0.69	
			glycolate	0.2	
			gluconate	0.1	
			formate	0.96	
5 *	0.1	105 °C	lactate	1.01	2.03
			formate	5.66	
			glycolate	0.11	
			acetate	0.37	
5	0.1	105 °C	lactate	1.01	1.89
			formate	5.23	
			glycolate	0.10	
			acetate	0.26	
6 *	1	105 °C	lactate	0.73	1.55
			formate	2.80	
			acetate	3.21	
6	1	105 °C	lactate	0.63	1.14
			formate	2.58	
			acetate	1.12	
7 *	0.1	140 °C	glucose	trace	2.34
			lactate	2.32	
			formate	10.18	
			glycolate	0.29	
			acetate	0.92	
7	0.1	140 °C	glucose	trace	2.02
			lactate	2.30	
			formate	10.11	
			glycolate	0.29	
			acetate	0.92	
8 *	1	140 °C	lactate	1.31	2.24
			formate	4.96	
			glycolate	0.4	
			acetate	1.01	
8	1	140 °C	lactate	1.05	1.67
			formate	4.02	
			glycolate	0.13	
			acetate	1.0	

* before photocatalytic reaction.

Glucose is a well-known substrate used for photocatalytic hydrogen evolution [54–56]. As such, in this research, the glucose molecules should act as electron donors in the

photocatalytic system, and should be oxidized by the photogenerated holes to form formate, gluconate, lactate, glycolate, or acetate anions. However, in such a case, the glucose should be consumed, and its concentration should decrease. Cellulose and starch have been shown to undergo depolymerization under the conditions of photocatalysis [27]. This process can provide additional glucose during photocatalytic hydrogen evolution. Additionally, in alkaline solutions, glucose is present mostly in its deprotonated form, $C_6H_{11}O_6^-$ [34]. $Cd_{1-x}Zn_xS$ photocatalysts have been shown in the literature to have hydroxyl groups on their surface under basic conditions, and $C_6H_{11}O_6^-$ species are adsorbed on the photocatalyst's surface through hydroxyl groups; more details are described elsewhere [57]. Once adsorbed, the glucose ions react with h+ to produce oxidized products, while simultaneously, the electrons reduce the number of protons, leading to hydrogen formation [34,58].

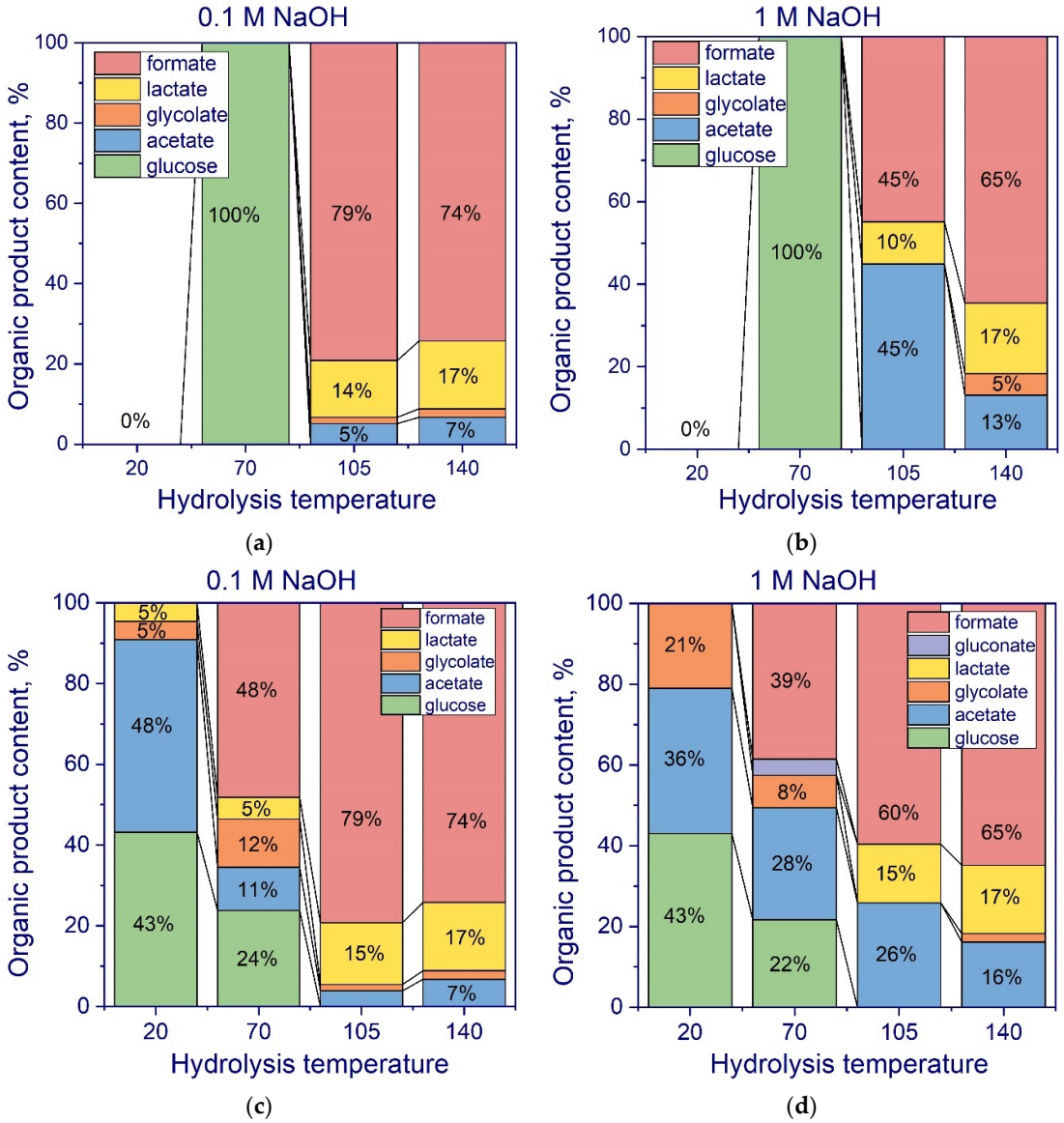

Figure 6. The dependence of organic compound distribution on the pretreatment temperature before (**a**,**b**) and after (**c**,**d**) H_2 evolution reaction. T = 20 °C in the case of no pretreatment; C_0(NaOH) = 0.1 M (**a**,**c**) and 1 M (**b**,**d**).

Additionally, total organic carbon (TOC) was measured for all reaction solutions (Figure 7). The high concentration of alkaline (1 M) led to the highest value of TOC at 20 °C and 70 °C, and the TOC content was lower following high-temperature (105 °C and 140 °C) hydrolysis. In contrast, for 0.1 M solutions of NaOH, the TOC value increased with the increase in temperature, but the highest value obtained at 140 °C was lower than that obtained in 1 M NaOH at 20 °C. These results confirm that a high alkaline concentration facilitates more extended starch hydrolysis. After the photocatalytic reaction, when the hydrolysates were obtained without thermal treatment or with treatment at 70 °C at a high alkali concentration, the TOC remained almost unchanged. In the case of the treatment at a low alkali concentration, the TOC remarkably increased. This can be explained by the fact that glucose is oxidized when hydrogen is released, but starch is also hydrolyzed with the release of glucose. In this way, the simultaneous production of hydrogen and valuable organic compounds is achieved by means of starch photoreforming under visible light irradiation. For hydrolysates obtained at high temperatures, the TOC content fell slightly after the photocatalytic reaction as the photocatalytic oxidation of light organic compounds into CO_2 likely occurred, given that dissolved oxygen was present in the reaction suspension in trace amounts.

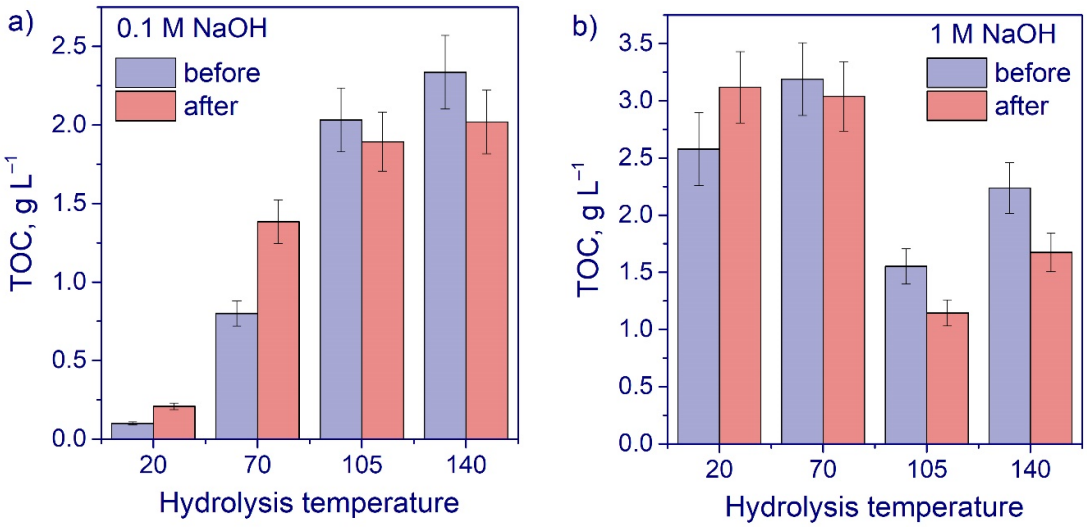

(**a**) (**b**)

Figure 7. TOC content in reaction mixture before and after photocatalytic reaction at different hydrolysis temperatures for 0.1 M NaOH (**a**) and 1 M NaOH (**b**) solutions.

Thus, a simple pretreatment in combination with photocatalysis makes it possible to obtain hydrogen and valuable organic compounds from practically insoluble corn starch.

3. Materials and Methods

3.1. Photocatalyst Synthesis

The following reagents were used for the synthesis and photocatalytic tests without purification: $CdCl_2 \cdot 2.5H_2O$ (Vekton, Russia, 98%), $Zn(NO_3)_2 \bullet 6H_2O$ (Acros Organics, Belgium, 98%), $Na_2S \bullet 6H_2O$ (Sigma-Aldrich, USA, 60%), H_2PtCl_6 (Reakhim, Russia, 98%), $NaBH_4$ (Acros Organics, Belgium, 98%), sodium hydroxide (Sigma-Aldrich, 98%), corn starch (Sigma-Aldrich, USA), and rice starch (Sigma-Aldrich, USA). The photocatalyst 0.5 wt. %$Pt/Cd_{0.7}Zn_{0.3}S/ZnS$ was synthesized via a simple two-stage technique including the deposition of a sulfide of cadmium and zinc throughout the intermediate stage of hydroxide formation. At the first stage, mixture of 0.1M solutions of $CdCl_2 \cdot$ and $Zn(NO_3)_2$ with a total volume of 100 mL (Cd/Zn = 3:7) interacted with 0.1 M NaOH solution (100 mL). Then,

250 mL of 0.1 M Na_2S was added to the hydroxide suspension under continuous stirring and a yellow-orange precipitate of Cd and Zn sulfide solid solution (~1 g) was obtained. After the washing and drying of the obtained sample, platinum (0.5 wt.%) was deposited via the reduction of the metal from a H_2PtCl_6 solution using $NaBH_4$. The synthesis procedure was described in detail in our previous work [35].

3.2. Photocatalyst Characterization

The obtained catalysts were characterized by various techniques, including UV–vis diffuse reflectance spectroscopy, X-ray diffraction (XRD), and X-ray photoelectron spectroscopy (XPS). The diffuse reflectance UV–vis spectra were obtained using a Shimadzu UV-2501 PC spectrophotometer with an ISR-240A diffuse reflectance unit.

The phase composition of the synthesized samples was determined by X-ray diffraction (XRD). The XRD patterns were recorded on a Bruker D8 diffractometer (Bruker, Germany) using CuKα radiation. Diffraction patterns were performed in the 2Θ range from 20 to 70° with a scanning step of 0.05° and an accumulation time of each point of 10 s. The calculation of the lattice constants and average crystallite sizes was carried out using the TOPAS software. The value of the parameter x in Cd1−xZnxS was determined using Vegard's law.

The X-ray photoelectron spectra were recorded on a SPECS spectrometer (SPECS, Germany) using AlKα radiation (h* = 1486.6 eV, 200 W). The binding energy of measured spectra was calibrated by the position of the Au$4f_{7/2}$ (BE = 84.0 eV) and Cu$2p_{3/2}$ (BE = 932.67) peaks.

The structure and microstructure of the photocatalysts were studied by HRTEM using a ThemisZ electron microscope (Thermo Fisher Scientific, TFS, USA) operated at an accelerating voltage of 200 kV. The microscope was equipped with a corrector of spherical aberrations, which provided a maximum lattice resolution of 0.06 nm, and a SuperX spectrometer (Thermo Fisher Scientific, TFS, USA). Images were recorded using a Ceta 16 CCD sensor (Thermo Fisher Scientific, TFS, USA). For electron microscopy studies, samples were deposited on perforated carbon substrates attached to aluminum grids using an ultrasonic dispersant.

3.3. Photocatalytic Activity Measurements

The method used for the activity test was described elsewhere [34]. Briefly, the reaction of hydrogen evolution was carried out in a sealed batch reactor containing an aqueous suspension of a photocatalyst and starch under irradiation. In this study, we used a 450 nm LED with a light intensity of 14 mW cm^{-2} and a light spot area of 19.6 cm^2. For some experiments, the starch was previously heated in a NaOH solution at 70, 105, or 140 °C for 1 h. After cooling to room temperature, the obtained mixture was placed in the reactor with the photocatalyst and photocatalytic activity tests were carried out. The amount of hydrogen evolved was measured by means of a gas chromatograph (Khromos, Russia).

The following equation was used to calculate the apparent quantum efficiency [34]:

$$AQE = 2 \times \frac{W_0(H_2)}{N_{phot}}, \quad (1)$$

where W is the rate of hydrogen formation in μmol·min^{-1} and N_{phot} is the calculated photon flux equal to 69 μE min^{-1}.

The study of organic products in the reaction solution was conducted by high-performance liquid chromatography (HPLC) using a Prominence LC-20 chromatograph (Shimadzu, Japan). The total organic carbon (TOC) was determined using a Multi N/C 2100S carbon and nitrogen analyzer (Analytik Jena, Germany). More details are described in our previous work [59].

4. Conclusions

In this research, a $PtO_x/Cd_{0.7}Zn_{0.3}S/ZnS$ nanocomposite photocatalyst was synthesized and tested in the photoreforming of corn starch with simultaneous hydrogen evolution under visible light irradiation. The influence of the starch's pretreatment conditions (sodium hydroxide concentration and temperature) on the reaction rate and organic products produced was studied. It was shown that the thermal treatment of an alkaline starch suspension leads to an increase in the hydrogen production rate owing to starch hydrolysis with glucose formation. The highest rate of H_2 evolution was obtained in a starch suspension in a 5 M solution of NaOH treated at 70 °C, yielding 730 $\mu mol \bullet h^{-1} \bullet g^{-1}$ with AQE = 1.8% at λ = 450 nm. However, further increasing the pretreatment temperature to 105 and 140 °C led to the near-complete inhibition of the formation of hydrogen from the hydrolysate.

For the first time, we have carried out a systematic investigation of the products of starch photoreforming accompanied by H_2 evolution. Glucose and gluconate, acetate, formate, glycolate, and lactate anions were found in the aqueous phase of the reaction mixture after the photocatalytic reaction. Thus, we have shown for the first time that the photocatalytic evolution of hydrogen from starch suspensions over a $Cd_{1-x}Zn_xS$-based photocatalyst under visible light is accompanied by the formation of valuable organic compounds.

Author Contributions: A.Y.K.: Investigation, data curation, visualization, writing—original draft preparation; T.B.M.: Data curation, formal analysis; N.V.G.: Data curation, formal analysis; A.V.B.: Data curation, formal analysis; E.Y.G.: Data curation, visualization; S.V.C.: Data curation, formal analysis; E.A.K.: Writing—original draft preparation, supervision, project administration, funding acquisition. All authors have read and agreed to the published version of the manuscript.

Funding: This research was funded by RFBR, project number 19-33-90110, and by the Ministry of Science and Higher Education of the Russian Federation within the governmental order for Boreskov Institute of Catalysis (project AAAA-A21-121011390009-1).

Data Availability Statement: The data presented in this study are available on request from the corresponding author.

Acknowledgments: The characterization experiments were performed using facilities of the shared research center "National center for investigation of catalysts" at Boreskov Institute of Catalysis. The authors are grateful to T. Larina for the UV-vis measurements.

Conflicts of Interest: The authors declare no conflict of interest.

References

1. Acar, C.; Bicer, Y.; Demir, M.E.; Dincer, I. Transition to A New Era with Light-Based Hydrogen Production for A Carbon-Free Society: An Overview. *Int. J. Hydrog. Energy* **2019**, *44*, 25347–25364.
2. Abe, J.O.; Popoola, A.P.I.; Ajenifuja, E.; Popoola, O.M. Hydrogen Energy, Economy and Storage: Review and Recommendation. *Int. J. Hydrog. Energy* **2019**, *44*, 15072–15086, doi:10.1016/j.ijhydene.2019.04.068.
3. Dincer, I.; Acar, C. Review and Evaluation of Hydrogen Production Methods for Better Sustainability. *Int. J. Hydrog. Energy* **2015**, *40*, 11094–11111, doi:10.1016/J.IJHYDENE.2014.12.035.
4. Nikolaidis, P.; Poullikkas, A. A Comparative Overview of Hydrogen Production Processes. *Renew. Sustain. Energy Rev.* **2017**, *67*, 597–611, doi:10.1016/J.RSER.2016.09.044.
5. Wang, M.; Liu, M.; Lu, J.; Wang, F. Photo Splitting of Bio-Polyols and Sugars to Methanol and Syngas. *Nat. Commun.* **2020**, *11*, 1–9, doi:10.1038/s41467-020-14915-8.
6. Peng, S.-Q.; Peng, Y.-J.; Li, Y.-X.; Lu, G.-X.; Li, S.-B. Photocatalytic Hydrogen Generation Using Glucose as Electron Donor over Pt/CdxZn1−xS Solid Solutions. *Res. Chem. Intermed.* **2009**, *35*, 739–749, doi:10.1007/s11164-009-0091-z.
7. Yasuda, M.; Matsumoto, T.; Yamashita, T. Sacrificial Hydrogen Production over TiO2-Based Photocatalysts: Polyols, Carboxylic Acids, and Saccharides. Renew. *Sustain. Energy Rev.* **2018**, *81*, 1627–1635, doi:10.1016/J.RSER.2017.05.243.
8. Ramis, G.; Bahadori, E.; Rossetti, I. Design of Efficient Photocatalytic Processes for the Production of Hydrogen from Biomass Derived Substrates. *Int. J. Hydrog. Energy* **2020**, *46*, 12105–12116 doi:10.1016/j.ijhydene.2020.02.192.
9. Puga, A.V. Photocatalytic Production of Hydrogen from Biomass-Derived Feedstocks. *Coord. Chem. Rev.* **2016**, *315*, 1–66, doi:10.1016/j.ccr.2015.12.009.

10. Nguyen, V.-C.; Ke, N.-J.; Nam, L.D.; Nguyen, B.-S.; Xiao, Y.-K.; Lee, Y.-L.; Teng, H. Photocatalytic Reforming of Sugar and Glucose into H2 over Functionalized Graphene Dots. *J. Mater. Chem. A* **2019**, *7*, 8384–8393, doi:10.1039/C8TA12123K.
11. Kondarides, D.I.; Daskalaki, V.M.; Patsoura, A.; Verykios, X.E. Hydrogen Production by Photo-Induced Reforming of Biomass Components and Derivatives at Ambient Conditions. *Catal. Lett.* **2008**, *122*, 26–32, doi:10.1007/s10562-007-9330-3.
12. Kandiel, T.A.; Ivanova, I.; Bahnemann, D.W. Long-Term Investigation of the Photocatalytic Hydrogen Production on Platinized TiO_2: An Isotopic Study. *Energy Environ. Sci.* **2014**, *7*, 1420–1425.
13. Puga, A.V.; Forneli, A.; García, H.; Corma, A. Production of H 2 by Ethanol Photoreforming on Au/TiO_2. *Adv. Funct. Mater.* **2014**, *24*, 241–248, doi:10.1002/adfm.201301907.
14. Taboada, E.; Angurell, I.; Llorca, J. Dynamic Photocatalytic Hydrogen Production from Ethanol-Water Mixtures in An Optical Fiber Honeycomb Reactor Loaded with Au/TiO_2. *J. Catal.* **2014**, *309*, 460–467, doi:10.1016/j.jcat.2013.10.025.
15. Patsoura, A.; Kondarides, D.I.; Verykios, X.E. Photocatalytic Degradation of Organic Pollutants with Simultaneous Production of Hydrogen. *Catal. Today* **2007**, *124*, 94–102, doi:10.1016/j.cattod.2007.03.028.
16. Panagiotopoulou, P.; Karamerou, E.E.; Kondarides, D.I. Kinetics and Mechanism of Glycerol Photo-Oxidation and Photo-Reforming Reactions in Aqueous TiO_2 and Pt/TiO_2 Suspensions. *Catal. Today* **2013**, *209*, 91–98, doi:10.1016/j.cattod.2012.09.029.
17. Beltram, A.; Romero-Ocaña, I.; Josè Delgado Jaen, J.; Montini, T.; Fornasiero, P. Photocatalytic Valorization of Ethanol and Glycerol over TiO_2 Polymorphs for Sustainable Hydrogen Production. *Appl. Catal. A Gen.* **2016**, *518*, 167–175, doi:10.1016/j.apcata.2015.09.022.
18. Fujita, S.-i.; Kawamori, H.; Honda, D.; Yoshida, H.; Arai, M. Photocatalytic Hydrogen Production from Aqueous Glycerol Solution Using NiO/TiO_2 Catalysts: Effects of Preparation and Reaction Conditions. *Appl. Catal. B Environ.* **2016**, *181*, 818–824, doi:10.1016/j.apcatb.2015.08.048.
19. Kuehnel, M.F.; Reisner, E. Solar Hydrogen Generation from Lignocellulose. *Angew. Chemie Int. Ed.* **2018**, *57*, 3290–3296, doi:10.1002/anie.201710133.
20. Chen, X.; Shen, S.; Guo, L.; Mao, S.S. Semiconductor-Based Photocatalytic Hydrogen Generation. *Chem. Rev.* **2010**, *110*, 6503–6570, doi:10.1021/cr1001645.
21. Wu, X.; Fan, X.; Xie, S.; Lin, J.; Cheng, J.; Zhang, Q.; Chen, L.; Wang, Y. Solar Energy-Driven Lignin-First Approach to Full Utilization of Lignocellulosic Biomass under Mild Conditions. *Nat. Catal.* **2018**, *1*, 772–780, doi:10.1038/s41929-018-0148-8.
22. Wakerley, D.W.; Kuehnel, M.F.; Orchard, K.L.; Ly, K.H.; Rosser, T.E.; Reisner, E. Solar-Driven Reforming of Lignocellulose to H_2 with a CdS/CdOx Photocatalyst. *Nat. Energy* **2017**, *2*, 17021, doi:10.1038/nenergy.2017.21.
23. Speltini, A.; Gualco, F.; Maraschi, F.; Sturini, M.; Dondi, D.; Malavasi, L.; Profumo, A. Photocatalytic Hydrogen Evolution Assisted by Aqueous (Waste)Biomass under Simulated Solar Light: Oxidized g-C_3N_4 Vs. P25 Titanium Dioxide. *Int. J. Hydrog. Energy* **2019**, *44*, 4072–4078, doi:10.1016/j.ijhydene.2018.12.126.
24. Kasap, H.; Achilleos, D.S.; Huang, A.; Reisner, E. Photoreforming of Lignocellulose into H2 Using Nanoengineered Carbon Nitride under Benign Conditions. *J. Am. Chem. Soc.* **2018**, *140*, 11604–11607, doi:10.1021/jacs.8b07853.
25. Pichler, C.M.; Uekert, T.; Reisner, E. Photoreforming of Biomass in Metal Salt Hydrate Solutions. *Chem. Commun.* **2020**, *56*, 5743–5746, doi:10.1039/d0cc01686a.
26. Jaswal, R.; Shende, R.; Nan, W.; Shende, A. Photocatalytic Reforming of Pinewood (*Pinus ponderosa*) Acid Hydrolysate for Hydrogen Generation. *Int. J. Hydrog. Energy* **2017**, *42*, 2839–2848, doi:10.1016/j.ijhydene.2016.12.006.
27. Speltini, A.; Sturini, M.; Dondi, D.; Annovazzi, E.; Maraschi, F.; Caratto, V.; Profumo, A.; Buttafava, A. Sunlight-Promoted Photocatalytic Hydrogen Gas Evolution from Water-Suspended Cellulose: A Systematic Study. *Photochem. Photobiol. Sci.* **2014**, *13*, 1410–1419, doi:10.1039/c4pp00128a.
28. Zhang, W.; Shen, S.; Song, T.; Chen, X.; Zhang, A.; Dou, H. Insights into the Structure and Conformation of Potato Resistant Starch (Type 2) Using Asymmetrical Flow Field-Flow Fractionation Coupled with Multiple Detectors. *Food Chem.* **2021**, *349*, 129168, doi:10.1016/j.foodchem.2021.129168.
29. Luo, Y.; Liu, Q.; Liu, J.; Liu, X.; Zhao, S.; Hu, Q.; Song, W.; Liu, B.; Liu, J.; Ding, C. Effect of Starch Multi-Scale Structure Alteration on Japonica Rice Flour Functionality under Infrared Radiation Drying and Storage. *LWT* **2021**, *143*, 111126, doi:10.1016/j.lwt.2021.111126.
30. Shimura, K.; Yoshida, H. Heterogeneous photocatalytic hydrogen production from water and biomass derivatives. *Energy Environ. Sci.* 2011, *4*, 2467–2481, doi: 10.1039/c1ee01120k
31. Kozlova, E.A.; Parmon, V.N. Heterogeneous Semiconductor Photocatalysts for Hydrogen Production from Aqueous Solutions of Electron Donors. *Russ. Chem. Rev.* **2017**, *86*, 870–906, doi:10.1070/RCR4739.
32. Stavitskaya, A.V.; Kozlova, E.A.; Kurenkova, A.Y. ; Glotov, A.P.; Selischev, D.S.; Ivanov, E.V.; Kozlov, D.V.; Vinokurov, V.A.; Fakhrullin, R.F.; Lvov, Y.M. Ru/CdS Quantum Dots Templated on Clay Nanotubes as Visible-Light-Active Photocatalysts: Optimization of S/Cd Ratio and Ru Content. *Chem. Eur. J.* **2020**, *26*, 13085–13092, doi:10.1002/chem.202002192.
33. Tahir, M.; Tasleem, S.; Tahir, B. Recent Development in Band Engineering of Binary Semiconductor Materials for Solar Driven Photocatalytic Hydrogen Production. *Int. J. Hydrog. Energy* **2020**, *45*, 15985–16038.
34. Kurenkova, A.Y.; Markovskaya, D.V.; Gerasimov, E.Y.; Prosvirin, I.P.; Cherepanova, S.V.; Kozlova, E.A. New Insights into the Mechanism of Photocatalytic Hydrogen Evolution from Aqueous Solutions of Saccharides over CdS-Based Photocatalysts under Visible Light. *Int. J. Hydrog. Energy* **2020**, *45*, 30165–30177, doi:10.1016/j.ijhydene.2020.08.133.
35. Kurenkova, A.Y.; Kozlova, E.A. CdS-Based Photocatalyst for Hydrogen Evolution from the Cellulose Aqueous Suspension. *AIP Conf. Proc.* **2020**, *2301*, 040007, doi:10.1063/5.0032673.

36. Kozlova, E.A.; Gribov, E.N.; Kurenkova, A.Y.; Cherepanova, S.V.; Gerasimov, E.Y.; Kozlov, D.V. Synthesis of Multiphase Au/$Cd_{0.6}Zn_{0.4}S$/ZnS Photocatalysts for Improved Photocatalytic Performance. *Int. J. Hydrog. Energy* **2019**, *44*, 23589–23599, doi:10.1016/j.ijhydene.2019.07.081.
37. Christoforidis, K.C.; Fornasiero, P. Photocatalytic Hydrogen Production: A Rift into the Future Energy Supply. *ChemCatChem* **2017**, *9*, 1523–1544, doi:10.1002/cctc.201601659.
38. Kumaravel, V.; Mathew, S.; Bartlett, J.; Pillai, S.C. Photocatalytic Hydrogen Production Using Metal Doped TiO_2: A Review of Recent Advances. *Appl. Catal. B Environ.* **2019**, *244*, 1021–1064.
39. Fontelles-Carceller, O.; Muñoz-Batista, M.J.; Rodríguez-Castellón, E.; Conesa, J.C.; Fernández-García, M.; Kubacka, A. Measuring and Interpreting Quantum Efficiency for Hydrogen Photo-Production Using Pt-titania Catalysts. *J. Catal.* **2017**, *347*, 157–169, doi:10.1016/j.jcat.2017.01.012.
40. Imizcoz, M.; Puga, A.V. Assessment of Photocatalytic Hydrogen Production from Biomass or Wastewaters Depending on the Metal Co-Catalyst and Its Deposition Method on TiO_2. *Catalysts* **2019**, *9*, 584, doi:10.3390/catal9070584.
41. Cherepanova, S.; Markovskaya, D.; Kozlova, E. Identification of A Deleterious Phase in Photocatalyst Based on $Cd_{1-x}Zn_xS/Zn(OH)_2$ by Simulated XRD Patterns. *Acta Crystallogr. Sect. B Struct. Sci. Cryst. Eng. Mater.* **2017**, *73*, 360–368, doi:10.1107/S2052520617001664.
42. Croy, J.R.; Mostafa, S.; Hickman, L.; Heinrich, H.; Cuenya, B.R. Bimetallic Pt-Metal Catalysts for the Decomposition of Methanol: Effect of Secondary Metal on the Oxidation State, Activity, and Selectivity of Pt. *Appl. Catal. A Gen.* **2008**, *350*, 207–216, doi:10.1016/j.apcata.2008.08.013.
43. Chetyrin, I.A.; Bukhtiyarov, A.V.; Prosvirin, I.P.; Khudorozhkov, A.K.; Bukhtiyarov, V.I. In Situ XPS and MS Study of Methane Oxidation on the Pd–Pt/Al2O3 Catalysts. *Top. Catal.* **2020**, *63*, 66–74, doi:10.1007/s11244-019-01217-7.
44. Kozlova, E.A.; Lyulyukin, M.N.; Markovskaya, D.V.; Bukhtiyarov, A.V.; Prosvirin, I.P.; Cherepanova, S.V.; Kozlov, D.V. Photocatalytic CO2 Reduction over Ni-Modified Cd1−xZnxS-Based Photocatalysts: Effect of Phase Composition of Photocatalyst and Reaction Media on Reduction Rate and Product Distribution. *Top. Catal.* **2020**, *63*, 121–129, doi:10.1007/s11244-020-01233-y.
45. Sanders, A.F.H.; De Jong, A.M.; De Beer, V.H.J.; Van Veen, J.A.R.; Niemantsverdriet, J.W. Formation of Cobalt-Molybdenum Sulfides in Hydrotreating Catalysts: A Surface Science Approach. *Appl. Surf. Sci.* **1999**, *144–145*, 380–384, doi:10.1016/S0169-4332(98)00831-9.
46. Li, C.; Yang, X.; Yang, B.; Yan, Y.; Qian, Y. Growth of Microtubular Complexes as Precursors to Synthesize Nanocrystalline ZnS and CdS. *J. Cryst. Growth* **2006**, *291*, 45–51, doi:10.1016/j.jcrysgro.2006.02.050.
47. Markovskaya, D.V.; Kozlova, E.A.; Gerasimov, E.Y.; Bukhtiyarov, A.V.; Kozlov, D.V. New Photocatalysts Based on $Cd_{0.3}Zn_{0.7}S$ and $Ni(OH)_2$ for Hydrogen Production from Ethanol Aqueous Solutions under Visible Light. *Appl. Catal. A Gen.* **2018**, *563*, 170–176, doi:10.1016/j.apcata.2018.07.002.
48. Fujishima, A.; Rao, T.N.; Tryk, D.A. Titanium Dioxide Photocatalysis. J. *Photochem. Photobiol. C Photochem. Rev.* **2000**, *1*, 1–21, doi:10.1016/S1389-5567(00)00002-2.
49. Markovskaya, D.V.; Cherepanova, S.V.; Saraev, A.A.; Gerasimov, E.Y.; Kozlova, E.A. Photocatalytic Hydrogen Evolution from Aqueous Solutions of Na2S/Na2SO3 under Visible Light Irradiation on CuS/$Cd_{0.3}Zn_{0.7}S$ and $Ni_zCd_{0.3}Zn_{0.7}S_{1+z}$. *Chem. Eng. J.* **2015**, *262*, 146–155, doi:10.1016/j.cej.2014.09.090.
50. Preethi, V.; Kanmani, S. Photocatalytic hydrogen Production Using Fe_2O_3-Based Core Shell Nano Particles with ZnS and CdS. *Int. J. Hydrog. Energy* **2014**, *39*, 1613–1622, doi:10.1016/j.ijhydene.2013.11.029.
51. Kumar, P.; Barrett, D.M.; Delwiche, M.J.; Stroeve, P. Methods for Pretreatment of Lignocellulosic Biomass for Efficient Hydrolysis and Biofuel Production. *Ind. Eng. Chem. Res.* **2009**, *48*, 3713–3729, doi:10.1021/ie801542g.
52. Awatani, T.; Dobson, K.D.; McQuillan, A.J.; Ohtani, B.; Uosaki, K. In Situ Infrared Spectroscopic Studies of Adsorption of Lactic Acid and Related Compounds on the TiO_2 and CdS Semiconductor Photocatalyst Surfaces from Aqueous Solutions. *Chem. Lett.* **1998**, *27*, 849–850, doi:10.1246/cl.1998.849.
53. Fu, X.; Long, J.; Wang, X.; Leung, D.Y.C.; Ding, Z.; Wu, L.; Zhang, Z.; Li, Z.; Fu, X. Photocatalytic Reforming of Biomass: A Systematic Study of Hydrogen Evolution from Glucose Solution. *Int. J. Hydrog. Energy* **2008**, *33*, 6484–6491, doi:10.1016/J.IJHYDENE.2008.07.068.
54. Kampouri, S.; Stylianou, K.C. Dual-Functional Photocatalysis for Simultaneous Hydrogen Production and Oxidation of Organic Substances. *ACS Catal.* **2019**, *9*, 4247–4270, doi:10.1021/acscatal.9b00332.
55. Iervolino, G.; Vaiano, V.; Murcia, J.J.; Rizzo, L.; Ventre, G.; Pepe, G.; Campiglia, P.; Hidalgo, M.C.; Navío, J.A.; Sannino, D. Photocatalytic Hydrogen Production from Degradation of Glucose over Fluorinated and Platinized TiO_2 Catalysts. *J. Catal.* **2016**, *339*, 47–56, doi:10.1016/j.jcat.2016.03.032.
56. Gomathisankar, P.; Yamamoto, D.; Katsumata, H.; Suzuki, T.; Kaneco, S. Photocatalytic Hydrogen Production with Aid of Simultaneous Metal Deposition Using Titanium Dioxide from Aqueous Glucose Solution. *Int. J. Hydrog. Energy* **2013**, *38*, 5517–5524, doi:10.1016/j.ijhydene.2013.03.014.
57. Li, Y.; Gao, D.; Peng, S.; Lu, G.; Li, S. Photocatalytic Hydrogen Evolution over Pt/Cd0.5Zn0.5S from Saltwater Using Glucose as Electron Donor: An Investigation of the Influence of Electrolyte NaCl. *Int. J. Hydrog. Energy* **2011**, *36*, 4291–4297, doi:10.1016/j.ijhydene.2011.01.038.
58. Wang, X.; Zheng, X.; Han, H.; Fan, Y.; Zhang, S.; Meng, S.; Chen, S. Photocatalytic Hydrogen Evolution from Biomass (Glucose Solution) on Au/CdS Nanorods with Au3+ Self-Reduction. *J. Solid State Chem.* **2020**, *289*, 121495, doi:10.1016/j.jssc.2020.121495.
59. Kozlova, E.A.; Kurenkova, A.Y.; Gerasimov, E.Y.; Gromov, N.V.; Medvedeva, T.B.; Saraev, A.A.; Kaichev, V.V. Comparative Study of Photoreforming of Glycerol on Pt/TiO_2 and CuO_x/TiO_2 Photocatalysts under UV Light. *Mater. Lett.* **2021**, *283*, 128901, doi:10.1016/j.matlet.2020.128901.